Synthesis and characterization of substituted garnet and perovskite based lithium ion conducting solid electrolytes

María Abreu-Sepúlveda[1], Dominique E. Williams[1], Ashfia Huq[2], Chetan Dhital[2], Yunchao Li[3], M. Parans Paranthaman[3], Karim Zaghib[4], A. Manivannan[1,5]

[1]United States Department of Energy, NETL, Morgantown, WV 26507
[2] Chemical and Engineering Materials Division, Oak Ridge National Laboratory, Oak Ridge, TN 37831
[3] Chemical Sciences Division, Oak Ridge National Laboratory, Oak Ridge, TN 37831
[4]Hydro-Quebec, Quebec, Canada, J3X 1S1
[5]Mechanical and Aerospace Engineering, West Virginia University, Morgantown, WV 26507

Corresponding Author: manivana@netl.doe.gov

Abstract

Titanium, tantalum-substituted $Li_7La_3Zr_{2-x}A_xO_{12}$ (LLZO, A= Ta, Ti) garnets, and chromium-substituted $La_{(2/3)-x}Li_{3x}Ti_{1-y}Cr_yO_3$ (LLTO) perovskites were prepared by a conventional solid-state reaction and the Pechini processes. The desired crystal phases were obtained by varying the calcination temperature and time, as well as the substitution concentration. All samples indicated decomposition of the precursors when heated above 750°C and formation of the desired phase after heat treatment at higher temperatures. Neutron diffraction data shows the formation of a predominant cubic phase in the case of Ta-LLZO, and monoclinic phase with minor impurity phases for Cr-LLTO. Ionic conductivity for Ti-LLZO ($Li_7La_3Zr_{2-x}Ti_xO_{12}$, x=0.6), Ta-LLZO ($Li_7La_3Zr_{2-x}Ta_xO_{12}$, x=0.5), and Cr-LLTO ($La_{(2/3)-x}Li_{3x}Ti_{1-y}Cr_yO_3$, y= 0.1) at room temperature were found to be $5.21\cdot10^{-6}$ S cm^{-1}, $1.01\cdot10^{-6}$ S cm^{-1}, and $1.2\cdot10^{-4}$ S cm^{-1}, respectively. The activation energies of the compounds were determined from the Arrhenius plot and were 0.44 eV ($Ti_{0.6}$-LLZO), 0.54 eV ($Ta_{0.5}$-LLZO), and 0.20 eV ($Cr_{0.1}$-LLTO).

Keywords: solid electrolytes, garnet, perovskite, lithium-ion conduction, solid state lithium-ion battery

Introduction

All-solid-state lithium-ion (Li-ion) batteries have the potential to replace the current air/moisture sensitive organic electrolytes in order to advance the safety of next generation Li-ion batteries [1-2]. In solid electrolytes, Li-ions are introduced into the interstitial spaces in the lattice for charge balance causing ionic conductivity. Moreover, solid electrolytes also act as a separator between the anode and cathode, eliminating the need for existing polymer based separators, and therefore reducing the number of interfaces for better ion transport. Recent examples of promising solid electrolytes are garnet-type compounds with the formula $Li_7La_3M_2O_{12}$ and cubic compounds with the general formula $Li_{0.5}La_{0.5}MO_3$ that have shown good electrochemical properties such as high ionic conductivity and low electronic conductivity [1-7]. Synthesis and structural characterization of the related systems, namely, cubic $Li_7La_3M_2O_{12}$ (M = Hf, Sn, Zr) exhibit higher conductivity as compared to their tetragonal phase [3, 8–12]. Typical ionic conduction in ceramic compounds is caused by the movement of ionic point defects, which are enhanced with an increase in temperature, although ionic conductivity for $Li_7La_3Zr_2O_{12}$ (LLZO) and $La_{(2/3)-x}Li_{3x}TiO_3$ (LLTO) has been reported to be reasonably high at room temperatures largely due to their structural characteristics [13-16].

Cubic garnet LLZO synthesized at 1230°C was reported to have a reasonably high Li-ion conduction with good thermal and chemical stability [13]. The cubic framework of the LLZO coupled with three-dimensional interstitial spaces consisting of tetrahedral *24d*-A sites bridged by octahedral sites sharing opposite faces introduces Li-ions into the interstitial space for charge transfer, yielding high Li-ion conductivity [6]. Attempts to stabilize cubic LLZO by element substitution at the Zr site has been an important task for future applications as electrolyte in lithium-ion batteries due to its enhanced conductivity at room temperature caused by the increase in Li^+ mobile sites (octahedral sites).

In the case of LLTO, a conduction path for the Li-ions in the perovskite structure happens through the A sites, which are partially occupied by Li and La-ions. The first Li-ion conducting perovskite by hetero-valent substitution of La^{3+} by Li^+ cations in the A-site deficient perovskite $La_{2/3}TiO_3$ was

reported by Latie et al. [7]. Moreover, when the A and B sites are substituted with different ions, a three-dimensional ionic conduction in perovskite-type oxides could be developed [7, 15]. In addition, several studies were performed in order to understand better the details of the crystal structure, Li-ion concentration and synthesis methods [16-21]. Cubic and tetragonal $La_{2/3-x}Li_{3x}TiO_3$ phases (x≈0.11) have better Li-ion conductivities as compared to other crystal structure modifications [22].

In the present study, we have investigated three systems based on the garnet and perovskite types, titanium/tantalum doped LLZO and chromium doped LLTO, referred as Ti-LLZO, Ta-LLZO and Cr-LLTO, respectively. Substitution-induced transitions in crystal phases are a significant solid electrolyte property since Li^+ mobility and structure density are significantly affected for certain phases. The main aim of this work is to investigate the ionic conductivity due to Ta, Ti and Cr substitutions in LLZO and LLTO ceramic oxides and to understand the possible phase transitions, improvement in ionic conductivity and mechanical strength due to the elemental substitution in these systems. All of the studied compositions were characterized for their structure, phase transition behavior, and lithium ion conductivity with scanning electron microscopy (SEM), powder X-Ray diffraction (XRD), powder neutron diffraction, and electrochemical impedance spectroscopy (EIS).

Materials and Methods

Garnet (LLZO)

For the preparation of the LLZO compounds by a solid-state reaction, Li_2CO_3 (99% Alfa Aesar), La_2O_3 (99.99% Alfa Aesar Reacton), TiO_2 (99.6% from Alfa Aesar) and ZrO_2 (99% Sigma Aldrich) were used as the starting materials. To compensate lithium loss at higher temperatures during synthesis, the compounds were prepared with 10 wt. % excess lithium. The precursors were mixed in stoichiometric amounts with acetone (ACS reagent) in an agate mortar and ground continuously for one hour until a

fine homogeneous powder was obtained. The powders were calcined at 850°C and 1100°C for 12 hours each, ground and cold pressed under 3.5 tons for two minutes. Each pellet was finally sintered at 1000°C for 12 hours on a zirconia plate covered with excess bulk powder to avoid significant Li loss. For the synthesis of Ta-LLZO, Li_2CO_3 (99% Alfa Aesar); (10 wt.% excess), La_2O_3 (Alfa Aesar, treated at 950°C overnight), ZrO_2 (Alfa Aesar, 98%), and Ta_2O_5 (Alfa Aesar 99.85%) were mixed using a mortar and pestle and heat treated at 950°C for 12 hours. Similarly, Ti-LLZO was also prepared using Li_2CO_3 (99% Alfa Aesar); (10 wt.% excess), La_2O_3 (Alfa Aesar, treated at 950°C overnight), ZrO_2 (Alfa Aesar, 98%), and TiO_2 (Alfa Aesar 99.85%) and heat treated at 950°C for 12 hours after grinding using a mortar and pestle. Ball milling was also performed in order to minimize the impurity phases. For both Ti-LLZO and Ta-LLZO compounds, ball milling was performed for an hour after the first calcination step. The final product was ground again and pressed into pellets. These pellets were sintered at 950°C for 12 hours for Ti-LLZO and 1130°C for 24 hours for Ta-LLZO in an alumina crucible covered with bulk powder.

Perovskite (LLTO)

A set of Cr-LLTO compositions with Cr substitutions of 0.06 and 0.1 were prepared by the Pechini and solid state methods. Metal nitrates were dissolved in de-ionized water and mixed with stoichiometric amounts of citric acid (anhydrous, 99.5% from Alfa Aesar). Ammonium titanyl oxalate monohydrate (99.998% from Sigma) was used as the titanium precursor dissolved in highly concentrated nitric acid followed by sonication for 60 minutes. This solution was added drop-wise to the other solution under vigorous stirring to avoid any precipitation of TiO_2. The solution was heated to 65°C and ethylene glycol was added. After vigorous stirring at 65°C, a homogeneous gel was formed due to the slow evaporation of water. The beaker was transferred to a heating mantle and the temperature

of the reaction was allowed to increase above 130°C while forming a 3D polymeric structure by the reaction of citric acid with ethylene glycol. The beaker was placed in a drying oven at 120°C overnight after which the resulting material was crushed and calcined at 750°C for four hours to eliminate any excess carbonates present from the synthesis process. The powder was ground thoroughly for at least one hour and cold-pressed into pellets at 3.2 tons for 5 minutes and heat treated at 850, 950 and 1050°C in steps of 100°C for every four hours. To avoid further loss of lithium, the pellets were placed on a zirconia plate along with the bulk powder. Solid state synthesis was performed by mixing Li_2CO_3 (99% Alfa Aesar); (10 wt.% excess), La_2O_3 (Alfa Aesar, treated at 950°C overnight), TiO_2 (Alfa Aesar, 99.95%). These precursors were mixed in stoichiometric amounts with acetone (ACS reagent) in an agate mortar and ground continuously for one hour until a fine homogeneous powder was obtained. Ball milling was also performed for Cr-LLTO (one hour) after calcination at 850°C for 4 hours, ground and cold pressed under 3.5 tons for two minutes. Each pellet was finally sintered at 1050°C for 12 hours on a zirconia plate covered with excess bulk powder to avoid significant Li loss and used for conductivity measurements.

Characterization

Following the synthesis, all compounds were thoroughly characterized for phase formation/crystallinity with an X'pert PANalytical X-ray diffractometer with Cu-Kα radiation of λ=1.5418 Å. For the XRD measurements, the powders were placed on top of a 1 cm diameter Si disk sample holder. A scanning electron microscopy (SEM) was employed to monitor surface morphology of the prepared pellets before and after polishing. Three samples with nominal compositions $Li_7La_3Zr_{1.5}Ta_{0.5}O_{12}$ ($Ta_{0.5}$-LLZO), $La_{(2/3)-x}Li_{3x}Ti_{0.9}Cr_{0.1}O_3$ ($Cr_{0.1}$-LLTO) and $La_{(2/3)-x}Li_{3x}Ti_{0.94}Cr_{0.06}O_3$ ($Cr_{0.06}$-LLTO) were chosen for further characterization with neutron diffraction measurements. Time of flight (TOF) neutron diffraction measurements were performed at POWGEN powder diffractometer at the

Spallation Neutron Source (SNS), Oak Ridge National Laboratory. The data were collected with a central wavelength of 1.066 Å at both 300 K and 10 K. This facility covers a d-spacing range of 0.276 Å to 4.606 Å. For the impedance measurement, both polished pellet surfaces were sputtered with a layer of gold. The experiment was performed on VersaSTAT 4 (Princeton Applied Research) with an internal frequency response analyzer in the frequency range 1 to 10^6 Hz with amplitude of 50 mV. Temperature was ramped from 25 to 125 ˚C in increments of 25 ˚C and about 30 min were allowed for temperature equilibration after each temperature change. The experimental impedance data were fitted by an equivalent circuit of (R_gQ_g) $(R_{gb}Q_{gb})$ (Q_{el}), where R is the resistance, Q is the constant phase element, and the subscripts g, gb, and el refer to grain, grain-boundary, and blocking electrodes, respectively [14].

Results and discussion

Garnet (LLZO)

Figure 1 shows the XRD patterns for un-substituted and Ti/Ta-substituted LLZO. It was found that these compounds have a larger fraction of cubic garnet phase with minor impurity peaks. Refinement of neutron diffraction data for this sample indicates a major cubic (space group I a -3 d) phase with composition $Li_{6.03}La_3Zr_{1.5}Ta_{0.5}O_{12}$. Minority phases obtained from neutron diffraction analysis were found to be less than 7%, possibly belonging to Li_2CO_3 (PDF # 97-001-6713) and Li_2O_2 (PDF # 97-005-0658) or Li_2O (PDF # 97-002-2402). It is also possible that contamination with Al occurred due to the use of Alumina crucibles during the heat treatment [23]. The results of the refinements are presented in Table 1 and Figure 2. Due to similar scattering cross sections of Zr and Ta for neutrons, their occupancies are fixed to their nominal values in the refinement. The ionic conductivity and the activation energy were estimated to be 1.01 $x10^{-6}$ S cm^{-1} and 0.54 eV from the Nyquist and Arrhenius plots (Figure 3). These results are comparable to the values reported in the literature for Ta substituted

compounds [6, 25-27]. The possible reason for the low conductivity value reported in the literature could be due to the lower sintering temperature of the pellets in our experiments.

Neutron diffraction refinements were not performed for $Ti_{0.6}$-LLZO samples; however, XRD pattern shows the presence of a cubic phase, with minor impurity phases contributing to less than 7%. The ionic conductivity of this material was in the range of 5.21 $x10^{-6}$ S cm^{-1} for $Ti_{0.6}$ substitution. Figure 4a shows the Nyquist plot for $Ti_{0.6}$-LLZO. Activation energy for $Ti_{0.6}$-LLZO was determined to be 0.44 (as per Figure. 4b). As mentioned before, the cubic garnet is the preferred structure for room temperature Li-ion conduction due to its characteristic framework with three-dimensional Li interstitial spaces [6]. Previous literature reports on the incorporation of a 1.3 wt. % gain of Al from the alumina crucible that leads to the formation of the cubic garnet phase increasing the density and hence the conductivity [23]. The compactness of the grains can be seen in the SEM micrograph sown in Figure 5, for both LLZO and Ti-LLZO. The density of the pellets was in the order of 95 to 98%.

It is important to mention that immense care is needed after the synthesis of these oxides owing to their stability which is affected by moisture, CO_2 etc. It appears that these oxides form impurity phases with time when exposed to air and moisture. A separate study has to be performed on the stability of these oxides.

Perovskite (LLTO)

XRD patterns of the compounds are presented in Figure 6, which indicate a well-defined pattern corresponding to monoclinic LLTO phase. Combined Neutron and X-ray powder diffraction data analysis were performed on both chromium substituted LLTO samples with the Rietveld method and GSAS software [24] in order to understand the structure further. The occupancy of chromium was fixed to its nominal value in both samples. LLTO samples have perovskite structure (ABO_3) as the parent structure.

A perovskite structure can have different symmetries (cubic, orthorhombic, tetragonal, rhombohedral and monoclinic) depending upon the A or B site cation or the doping element of A or B site cation. Several possibilities with different symmetries were tried and the best fit that also accounts for all the observed reflection was obtained with the monoclinic structure (space group P 1 21/n1). To determine the site mixing for Li, four different models were investigated. These include doping A site (La site) or B site (Ti site) with Lithium [see Table 2 Models I to IV]. The analysis indicates that lithium most likely goes to the B site (Ti site) forming a composition close to $La[Li_{1/3}(Ti,Cr)_{2/3}]O_3$ with cubic $Li_{1-x}Ti_{1+x}O_2$ as the minority phase (about 4%, space group F m -3 m , a=b=c= 4.14Å, PDF #97-002-8323). The results of all the models are shown in Table 2 and Figures 7 and 8, along with their goodness of fit and atomic parameters. In the case of $Cr_{0.1}$-LLTO, the XRD pattern seems to be mostly matching with cubic phase after ball milling (PDF # 00-046-0465).

In the present study, we have observed that doping chromium in LLTO ($La_{(2/3)-x}Li_{3x}Ti_{1.9}Cr_{0.1}O_3$) also showed an improvement in the conductivity of 1.2 10^{-4} S cm^{-1} as well as good mechanical strength. The EIS value for $Cr_{0.1}$-LLTO is presented in Figure 9a. The activation energies of the LLTO and substituted-LLTO were found to be 0.32 and 0.20 eV, respectively. The higher conductivity value for the Cr substitution may be possible due to the existence of Cr^{4+} which could lead to electronic conductivity especially, at high temperature operations.

It is crucial that the compact sintering without any gaps in the grains of these oxides is required to achieve the best ionic conductivity. The SEM images of LLTO and $Cr_{0.1}$-LLTO are shown in Figure 10. The surface morphology indicates that the grains are well sintered together without any porosity, which enhances mechanical stability as well as the Li-ion conduction. The grain sizes of the pellets were about 1-6 μm. Polishing the pellets before performing the impedance measurements was needed in order to remove loosely bound particles. As indicated before, it is important to mention that over time that substituted as well as pure LLZO and LLTO samples degrade due to the reaction with moisture, oxygen,

CO_2 etc. in the environment and form impurity phases. The study of these materials aging/degradation processes is very important for reliable and fully functioning solid state lithium-ion battery in the future. Therefore, detailed experimental investigations are needed towards the understanding of any impurity phase formation over time due to the environmental conditions.

Conclusion

In summary, we have investigated the effect of B-site substitution in the phase formation and ionic conductivity for a family of ceramic oxides. Titanium and tantalum substituted $Li_7La_3Zr_2O_{12}$, and chromium substituted $La_{(2/3)-x}Li_{3x}TiO_3$ were prepared successfully by a solid-state reaction and Pechini methods respectively. Neutron diffraction and XRD powder patterns indicated the presence of a single phase even at high substitution concentrations at the B site after following appropriate heat treatment conditions. In general, this work showed an improved ionic conductivity of the compounds without compromising the stability of the high Li-ion conduction phases. Ionic conductivity values depend upon the grain boundaries, sintering temperatures and mechanical strength in addition to the crystal structure. Optimization of the Li concentration to achieve the highest Li-ion conductivity and the phase evolution via systematic substitution is currently in progress as well as studies for the effect of environmental conditions on the impurity phase formation.

Acknowledgements

This work was supported by the Vehicle Technology Program (EERE), the Oak Ridge Institute for Science and Education (ORISE) and Mickey Leland Energy Fellowship (MLEF) programs. A portion of this research at ORNL's Spallation Neutron Source was sponsored by the Scientific User Facilities Division, Office of Basic Energy Sciences, U.S. Department of Energy. Support (MPP and YL) for Neutron characterizations and impedance measurements was provided by U.S. Department of Energy, Office of Science, Office of Basic Energy Sciences, Division of Materials Sciences and Engineering.

References

[1] Fergus JW (2010) J Power Sources 195:4554

[2] Thangadurai V, Kaack H, Weppner W (2003) J Am Ceram Soc 86 [3]:437

[3] Murugan R, Thangadurai V, Weppner W (2008) App Phys A 91:615

[4] Murugan R, Weppner W, Schmid-Beurmann P, Thangadurai V (2007) Mater Sci Eng B143:14

[5] Murugan R, Thangadurai V, Weppner W (2007) Ionics 13:195

[6] Gupta A, Murugan R, Paranthaman M.P, Bi Z, Bridges CA, Nakanishi M, Sokolov AP, Han KS, Hagaman EW, Xie H, Mullins CB, Goodenough JB (2012) J Power Sources 209:184

[7] Latie L Villeneuve G, Conte D, Flem GL (1984) J Solid State Chem 51:293

[8] Zaib T, Ortnet M, Murugan R, Weppner W (2009) Ionics 16:855

[9] Awaka J, Kijima N, Kataoka K, Hayakawa H, Ohshima K, Akimoto J (2010) J Solid State Chem 183:180

[10] Percival J, Kendrick E, Smith R.I, Slater PR (2009) Dalton Trans 26:5177

[11] Rangasamy E, Wolfenstine J, and Sakamoto J (2012) Solid State Ionics 206:28

[12] Galven C, Fourquet JL, Crosnier-Lopez MP, Le Berre F (2011) Chem. Mater 23:1892

[13] Kumazaki S, Iriyama Y, Kim K-H, Murugan R, Tanabe K, Yamamoto K, Hirayama T, Ogumi Z, (2011) Electrochem Commun 13:509

[14] Murugan R, Thangadurai V, Weppner W (2007) Angewandte Chemie-International Ed 46:7778

[15] Belous AG, Novitskaya GN, Polyanetskaya SV, Gornikov YI (1987) Izv Akad Russ J Inorg Chem, 32:470

[16] Kawai H, Kuwano J (1994) J Electrochem Soc 141:L78

[17] Harada Y, Hirakoso Y, Kawai H, Kuwano J(1999) Solid State Ionics 121:245

[18] Inaguma Y, Itoh M (1996) Solid State Ionics 86-8:257

[19] Kunugi S, Inaguma Y, Itoh M (1999) Solid State Ionics 122:35

[20] Ibarra J, Varez A, Leon C, Santamaria J, Torres-Martinez LM, Sanz, J (2000) Solid State Ionics 134:219

[21] Ban CW, Choi GM (2001) Solid State Ionic 140:285

[22] Inaguma Y, Katsumata T, Itoh M, Morii Y (2002) J Solid State Chem 166:67 [18]

[23] Geiger CA, Alekseev E, Lazic B, Fisch M, Armbruster T, Langner R, Fechtelkord M, Kim N, Pettke T, Weppner W (2011) Inorg Chem 50:1089

[24] Toby BH (2001) J Applied Crystallography 34 (2):210

[25] Bi Z, Bridges CA, Kim J-H, Huq A, Paranthaman MP (2011) J Power Sources 196:7395

[26] Li Y, Wang C-A, Xie H, Cheng J, Goodenough JB (2011) Electrochem Commun 13:1289

[27] Li Y, Cao Y, Guo X (2013) Solid State Ionics 253:76 Zaib T, Ortnet M, Murugan R, Weppner W (2009) Ionics 16:855

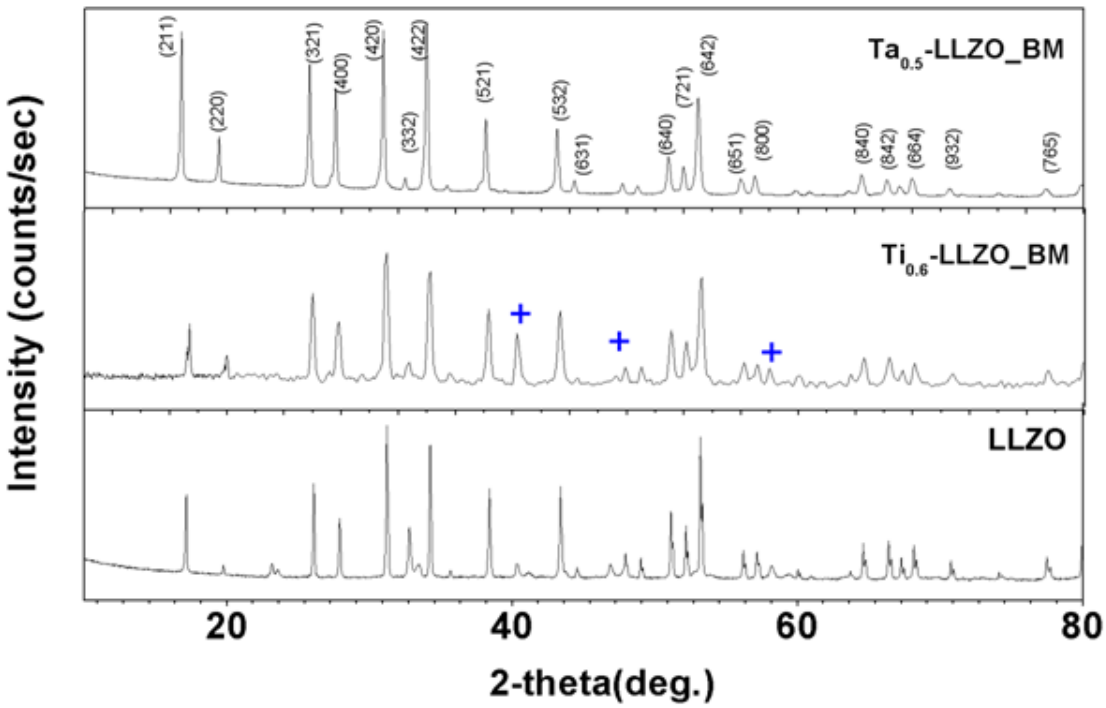

Figure 1. XRD patterns for $Li_7La_3Zr_2O_{12}$ (LLZO), $Li_7La_3Zr_{1.4}Ti_{0.6}O_{12}$ ($Ti_{0.6}$-LLZO) and $Li_7La_3Zr_{1.5}Ta_{0.5}O_{12}$ ($Ta_{0.5}$-LLZO) matching with cubic garnet (PDF# 97-026-1302). Impurity phases denoted by + possibly belonging Li_2O_2 (PDF# 97-005-0658). BM refers to ball milling during synthesis. The lattice constants for LLZO, $Ti_{0.6}$-LLZO and $Ta_{0.5}$-LLZO were found to be: 12.95 Å, 12.93 Å, and 12.96 Å, respectively.

Table 1. Fitting parameters from the neutron diffraction model for $Li_7La_3Zr_{1.5}Ta_{0.5}O_{12}$*.

Atom	x	y	z	100 × U_{iso}(Å^2)	Occupancy
La1	0.125	0	0.25	0.796(16)	1
Ta1	0	0	0	0.588(19)	0.25
Zr1	0	0	0	0.588(19)	0.75
Li1	0.25	0.875	0	2.91(35)	0.573(37)
Li2	0.1038(6)	0.6872(7)	0.5750(7)	1.54(25)	0.359(15)
O1	0.28110(8)	0.10143(9)	0.19634(9)	1.175(19)	1

*Major phase: $Li_{6.036}La_3Zr_{1.533}Ta_{0.465}O_{12}$ (space group I a -3 d), a = b = c = 12.93750(8) Å; wt. fraction: 0.93604(35)
Minor phase: Li_2CO_3 (space group C2/c), a = 8.3617(11) Å, b = 4.9744(5) Å, c = 6.1965(7) Å, α = 90 β = 114.7(3) γ = 90; wt. fraction: 0.638(1)

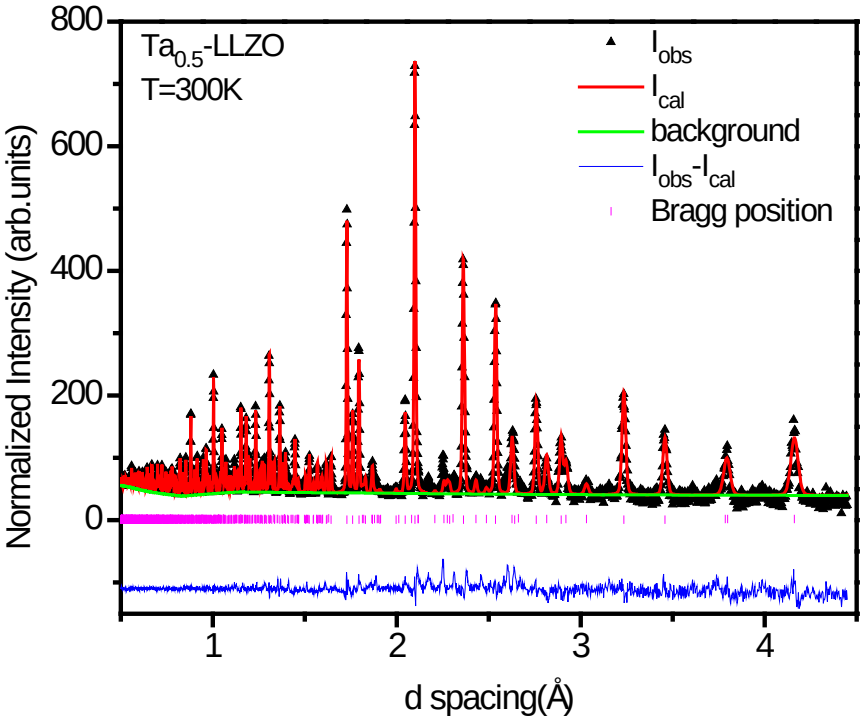

Figure 2. Rietveld refinement of the neutron diffraction data for $Ta_{0.5}$-LLZO.

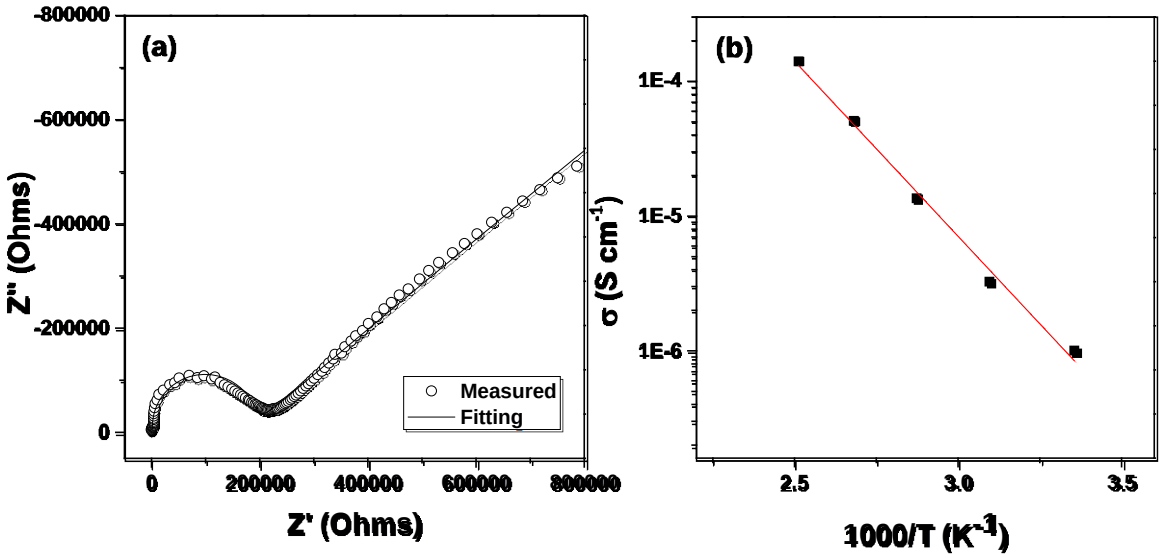

Figure 3. (a) Nyquist plot for $Ta_{0.5}$-LLZO at room temperature; (b) Arrhenius plot for $Ta_{0.5}$-LLZO at high temperatures.

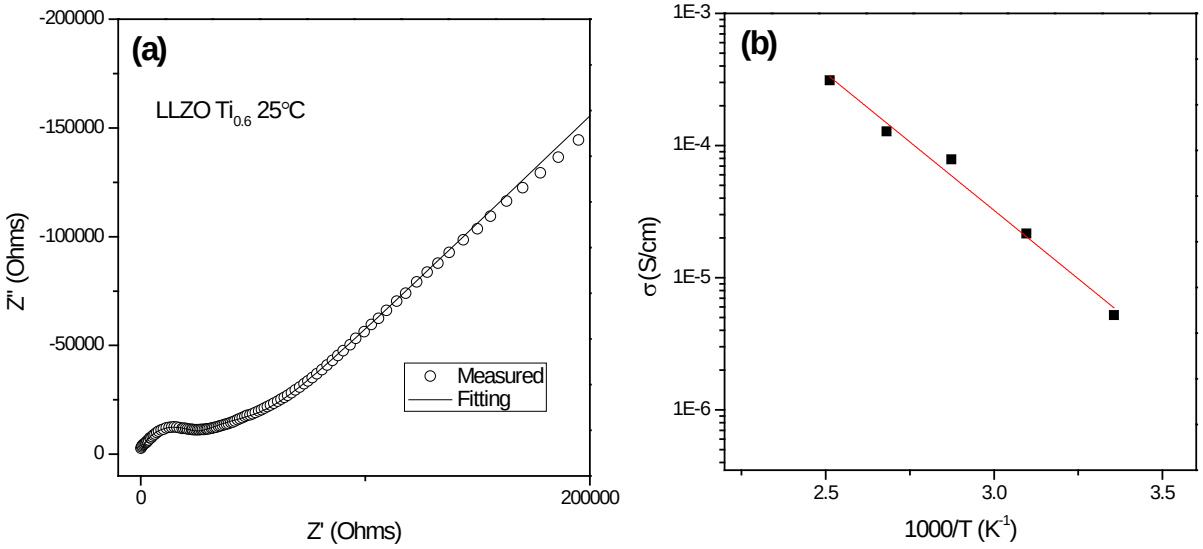

Figure 4. (a) Nyquist plot for $Ti_{0.6}$-LLZO at room temperature; (b) Arrhenius plot for $Ti_{0.6}$ -LLZO at high temperatures.

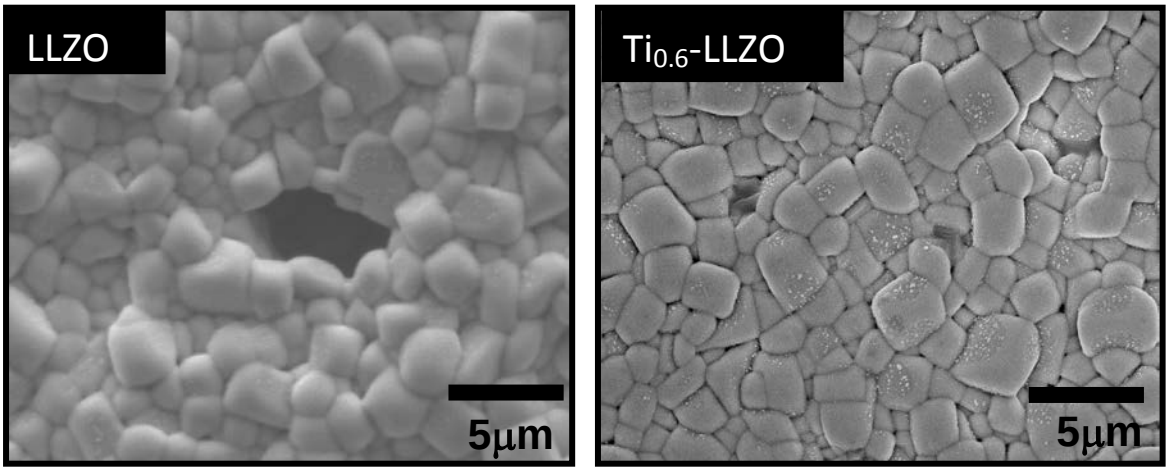

Figure 5. SEM micrographs of LLZO and $Ti_{0.6}$-LLZO.

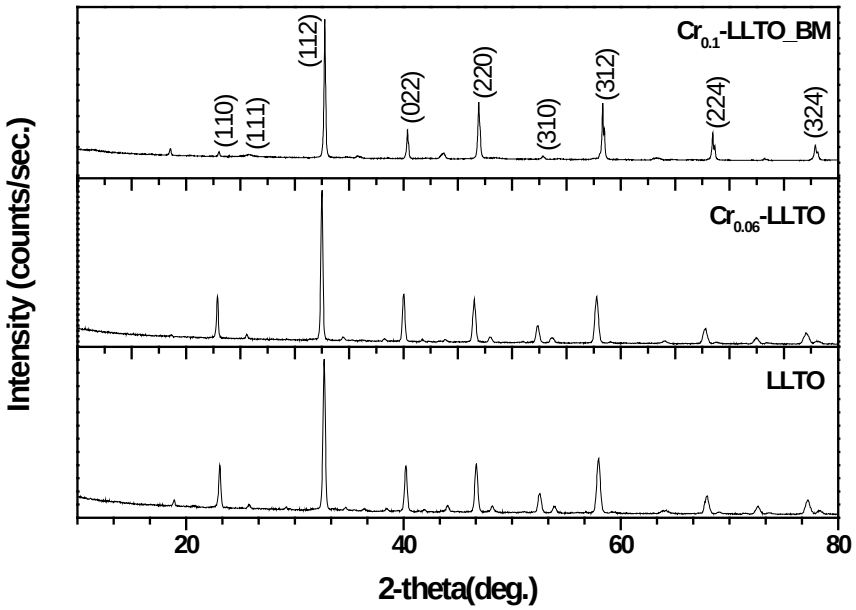

Figure 6. XRD patterns of LLTO, $Cr_{0.06}$-LLTO matching with monoclinic phase (PDF # 01-070-9361), and $Cr_{0.1}$-LLTO matching with cubic phase (PDF # 00-046-0465) with minor peaks corresponding to monoclinic phase. Lattice constants were determined to be: a= 5.56 Å, b= 5.56 Å, c= 9.60 Å (LLTO); a= 5.54 Å, b= 5.54 Å, c= 9.63 Å ($Cr_{0.06}$-LLTO); and a= 3.85 Å, b= 3.85 Å, c= 3.85 Å ($Cr_{0.1}$-LLTO). BM refers to ball milled.

Table 2. Parameters of the models fitting $Cr_{0.06}$-LLTO.

[**Note**: The Tables show the data at T = 300K, low temperature data also gave similar results]

Model I: R_{wp} = 0.027, χ2 = 1.104*[+]					
Atom	**x**	**y**	**z**	**100 × U_{iso}(Å^2)**	**Occupancy**
La1	0.4940(5)	0.53377(23)	0.2492(8)	0.805(25)	1
Ti1	0.5	0	0	0.81(22)	0.94
Ti2	0	0.5	0	0.32(15)	0.223(50)
Li1	0	0.5	0	0.32(15)	0.78(5)
O1	0.2833(9)	0.2896(14)	0.0388(6)	0.87(8)	1
O2	0.2152(11)	0.7831(15)	0.0386(7)	1.28(10)	1
O3	0.5752(5)	0.9863(4)	0.2527(8)	0.86(4)	1
Cr1	0.5	0	0	0.81(22)	0.06

***Major phase**: $Li_{0.247}(6)LaTi_{0.723}(3)Cr_{0.03}O_3$ **(**space group P 1 21/n1**)**
a = 5.55662(12) Å, b = 5.56899(12) Å, c = 7.84194(15) Å, α = 90 β = 89.8832(25) γ = 90
wt. fraction:0.9688(4)
[+]Minority phases may be cubic TiO and/or $Li_{1-x}Ti_{1+x}O_2$

Model II: R_{wp} = 0.0276, χ2=1.115*					
Atom	**x**	**y**	**z**	**100 × U_{iso}(Å^2)**	**Occupancy**
La1	0.4944(5)	0.53364(24)	0.2496(8)	0.796(24)	1
Ti1	0.5	0	0	0.5	0.518(32)
Ti2	0	0.5	0	1.38(11)	0.94

Li1	0	0.5	0	0.5	0.482(32)
O1	0.2827(9)	0.2909(15)	0.0387(6)	0.88(9)	1
O2	0.2141(10)	0.7823(15)	0.0384(7)	1.22(10)	1
O3	0.5750(5)	0.9862(4)	0.2530(7)	0.87(4)	1
Cr2	0	0.5	0	1.38(11)	0.06

***Major phase**: $Li_{0.224}(5)LaTi_{0.746}(5)Cr_{0.03}O_3$ **(**space group P 1 21/n1**)**
a = 5.55662(12) Å, b = 5.56899(12) Å, c = 7.84194(15) Å, α = 90 β = 89.8832(25) γ = 90
wt. fraction:0.96902(38)

(Continuation Table 2)

Model III: R_{wp} = 0.0302, χ2=1.333*

Atom	**x**	**y**	**z**	**100 × U_{iso}(Å^2)**	**Occupancy**
La1	0.4931(4)	0.53382(24)	0.2476(7)	0.5	0.944(5)
Ti1	0.5	0	0	2.51(13)	1
Ti2	0	0.5	0	0.5	0.94
Li1	0.4931(4)	0.53382(24)	0.2475(7)	0.5	0.056(5)
O1	0.2826(10)	0.2865(14)	0.0386(7)	0.91(10)	1
O2	0.2132(11)	0.7864(13)	0.0385(7)	1.35(10)	1
O3	0.5749(5)	0.9871(4)	0.2524(8)	0.90(4)	1
Cr2	0	0.5	0	0.5	0.06

***Major phase**: $Li_{0.000}(4)La_{1.000}(4)Ti_{0.97}Cr_{0.03}O_3$**(**space group P 1 21/n1**)**
a = 5.55662(12) Å, b = 5.56899(12) Å, c = 7.84194(15) Å, α = 90 β = 89.8832(25) γ = 90
wt. fraction:0.9695(4)

Model IV: R_{wp} = 0.028, χ2=1.101*

Atom	x	y	z	$100 \times U_{iso}(Å^2)$	Occupancy
La1	0.4943(5)	0.53375(24)	0.2490(8)	0.813(25)	1
Ti1	0.5	0	0	0.34(27)	0.08(13)
Ti2	0	0.5	0	0.76(27)	1.07(16)
Li1	0.5	0	0	0.34(27)	0.92(13)
O1	0.2812(9)	0.2863(12)	0.0385(6)	0.86(8)	1
O2	0.2130(10)	0.7868(13)	0.0390(7)	1.30(10)	1
O3	0.5752(5)	0.9861(4)	0.2531(7)	0.86(4)	1
Cr2	0	0.5	0	0.76(27)	0.06
Li2	0	0.5	0	0.76(27)	

***Major phase**: $Li_{0.264}(2)LaTi_{0.705}(2)Cr_{0.03}O_3$ **(**space group P 1 21/n1**)**
a = 5.55662(12) Å, b = 5.56899(12) Å, c = 7.84194(15) Å, α = 90 β = 89.8832(25) γ = 90
wt. fraction:0.9687(4)

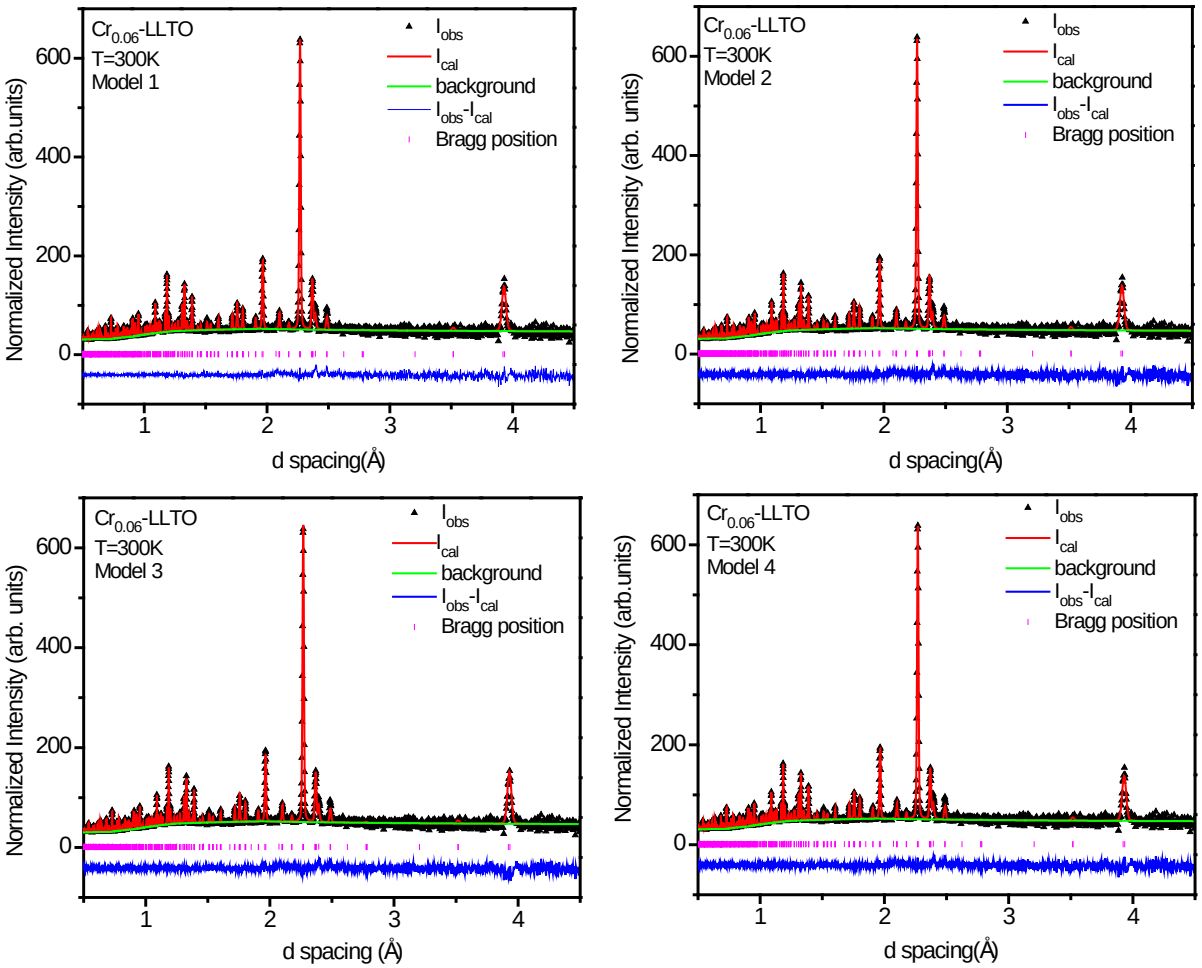

Figure 7. Rietveld refinement of the neutron diffraction data for $Cr_{0.06}$-LLTO as described in Table 2.

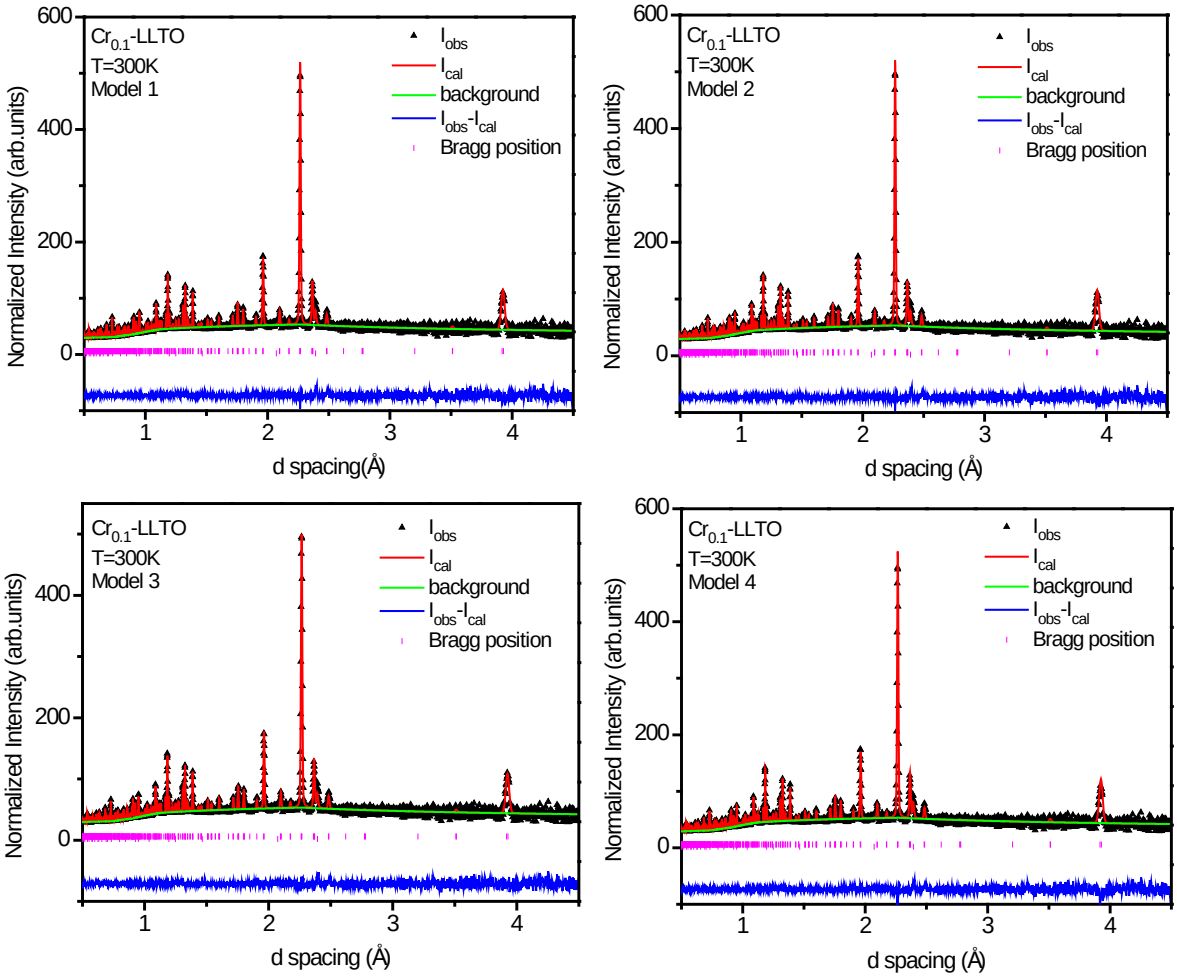

Figure 8. Rietveld refinement of the neutron diffraction data for $Cr_{0.1}$-LLTO following the parameters presented in Table 2.

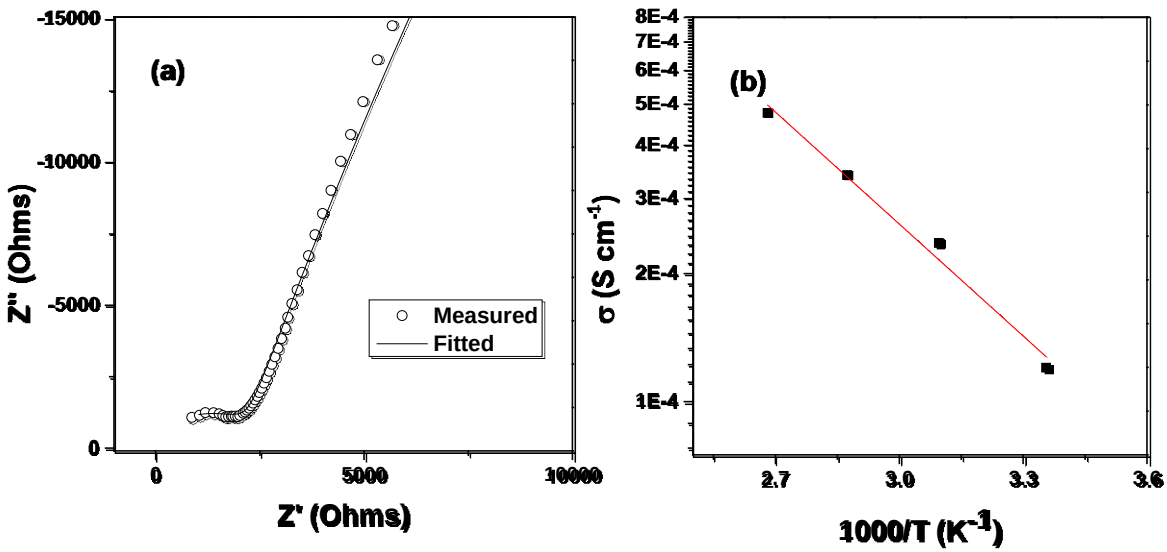

Figure 9. (a) Nyquist plot for $Cr_{0.1}$-LLTO at room temperature; (b) Arrhenius plot for $Cr_{0.1}$-LLTO at higher temperatures.

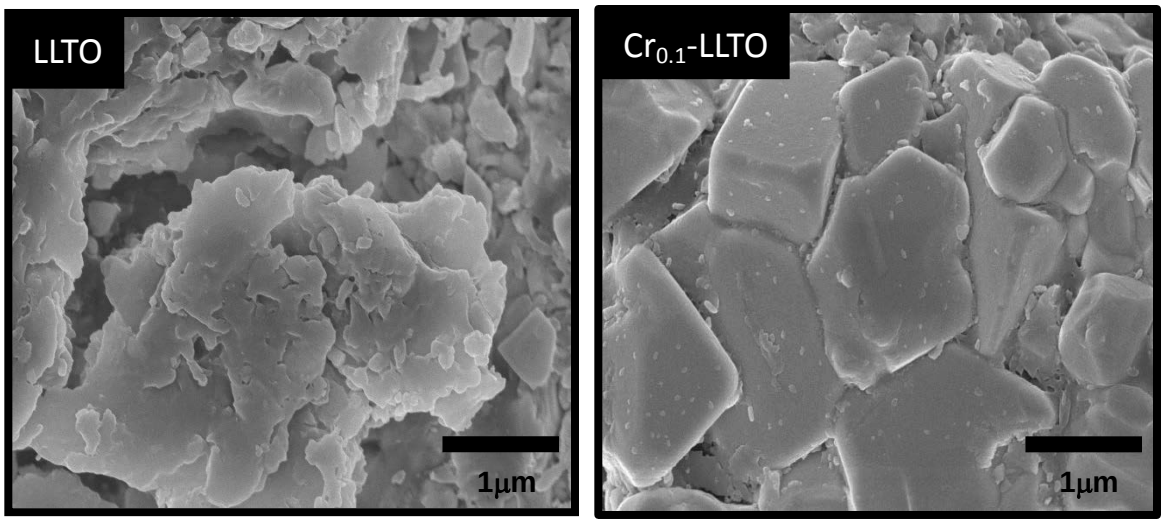

Figure 10. SEM micrograph of LLTO and $Cr_{0.1}$-LLTO.